SUPPLEMENTARY INFORMATION

"Persistence of full glacial conditions in the central Pacific until 15 thousand years ago"

P.-H. Blard, J. Lavé, R. Pik, P. Wagnon, D. Bourlès

1 - Geological and geomorphic settings of Mauna Kea

Volcanics of Mauna Kea (19°46'50 N, 155°290 E, Big Island) result from the Hawaiian hot spot activity. Basalts outcropping on the volcano flanks range in age from ~ 250 to 4 ka and can de divided in two distinct lithic units [S1]. The older unit (Hamakua volcanics, between ~250 and 65 ka old) are primarily alkali and transitional basalt that outcrop mainly over the lower slopes of the volcano (below 3000 m). These basalts are also exposed locally above 3200 m, on the Mauna Kea south-western slope, in the Pohakuloa gulch (Fig. 1). Indeed, most of the volcano upper flanks are covered by the overlying younger Laupahoehoe unit (~65 to 4 ka), whose petrology is dominated by aphyric hawaiite lavas and pyroclastic deposits. The last Mauna Kea ice cap was concomitant to this last eruptive unit. The summit configuration, characterized by inter-bedded glacial and volcanic formations, is therefore the result of these two time-overlapping events. Cosmogenic ^{3}He dating requires olivines (or pyroxenes) rich basalts. The Mauna Kea tills that are made of such appropriate rocks are however extremely rare over the upper slopes of the volcano [S1]. Glacial deposits filling these petrologic criteria were only encountered within the Pohakuloa gulch, where cobbles and boulders were sampled in the glacial formations M0 and M2a-b-c (Fig. 1c).

doi: 10.1038/nature06142

2 - Cosmogenic ^{3}He data

Sample	Object	Height (cm)	Mineral	Latitude	Longitude	Altitude (m)	$^{3}He_c$ [a] (10^6 at.g^{-1})	Shielding correction	Boulder correction	Paleomagnetic correction	Age[b] (ka)
Recessional moraines											
M2a											
MK9A	Boulder	50	Oli	19°47.67 N	155°29.74 W	3570	9.7 ± 0.3	0.97	0.93	0.94	12.1 ± 1.2
MK9B	Cobble	10	Oli	19°47.67 N	155°29.74 W	3570	8.0 ± 0.2	0.97	0.95	0.94	9.8 ± 1
MK9D	Cobble	20	Oli	19°47.67 N	155°29.74 W	3570	8.7 ± 0.3	0.97	0.95	0.94	*10.6 ± 1.1*
MK9D	Cobble	20	Cpx	19°47.67 N	155°29.74 W	3570	8.5 ± 0.3	0.97	0.95	0.94	
MK9F	Boulder	80	Oli	19°47.67 N	155°29.74 W	3570	11.9 ± 0.3	0.97	0.95	0.94	14.6 ± 1.5
M2b											
MK10A	Boulder	80	Cpx	19°47.65 N	155°29.71 W	3570	12.6 ± 0.4	0.97	0.93	0.94	15.7 ± 1.6
MK10B	Boulder	100	Oli	19°47.65 N	155°29.71 W	3570	15.5 ± 0.4	0.97	0.95	0.94	18.9 ± 1.9
MK10C	Boulder	120	Oli	19°47.65 N	155°29.71 W	3570	12.0 ± 0.4	0.97	0.93	0.94	14.9 ± 1.5
M2c											
MK11	Boulder	250	Oli	19°47.74 N	155°29.54 W	3590	11.4 ± 0.5	0.98	0.94	0.94	*14.5 ± 1.5*
MK11	Boulder	250	Cpx	19°47.74 N	155°29.54 W	3590	12.3 ± 0.4	0.98	0.94	0.94	
Terminal moraine M0											
MK12A	Boulder	100	Oli	19°47.045 N	155°30.091 W	3220	12.5 ± 0.4	1	0.95	0.97	17.2 ± 1.7
MK12B	Boulder	100	Oli	19°47.045 N	155°30.091 W	3190	13.6 ± 0.4	1	0.95	0.97	19.1 ± 1.9
MK12C	Boulder	100	Oli	19°47.045 N	155°30.091 W	3190	13.2 ± 0.4	1	0.95	0.97	18.6 ± 1.9
MK12C replicate	Boulder	100	Oli	19°47.045 N	155°30.091 W	3190	13.3 ± 0.4	1	0.95	0.97	

[a] $^{3}He_c$ concentrations are given with 1σ analytical uncertainty.
[b] Absolute computed ages are given with 10% uncertainty. Ages in italic are weighted means for single boulder or cobble (from 2 replicates for MK12C and 2 types of phenocrysts for MK9D and MK11).

Table S1 - Samples locations, cosmogenic ^{3}He data and corrected exposure ages

3 - Evaluation of the sampling strategy

In order to test the relative influences of post and pre-depositional processes [S2], boulders and cobbles sampled on the M2 moraines have been chosen with various diameters (ranging from 0.1 to 2.5 m), and their $^{3}He_c$ concentrations plotted *versus* their respective heights (Fig. S1). For cobbles smaller than ~80 cm diameter, $^{3}He_c$ concentrations increase monotonically with the cobble size, until reaching a *plateau* value for >80 cm sizes. Such an array can be interpreted as the result of the removal of till material by erosion, at a rate of 60±20 mm.kyr^{-1} (Fig. S1), inducing progressive exhumation of the smallest cobbles, whereas the tops of the highest boulders have been continuously exposed. According to this interpretation, the only dates provided by boulders larger than 80 cm have been considered to determine the age of M2 deposition.

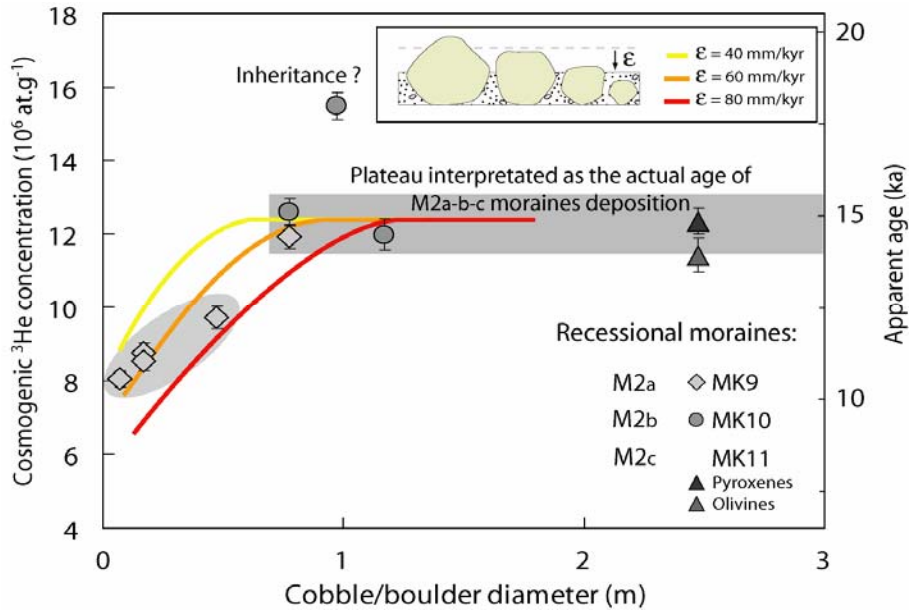

Fig. S1 - Plot of $^{3}He_c$ concentration *vs*. the cobbles/boulders size of the M2a-b-c recessional moraines

$^{3}He_c$ analytical uncertainties are 1σ. Assuming a plateau age of ~15 ka, a till matrix deflation rate between 40 and 80 mm.kyr^{-1} is required to fit the data. MK10B is on the contrary characterized by $^{3}He_c$ value being 25% above the plateau concentration, and is thus supposed to bear inherited cosmogenic ^{3}He accumulated before the moraine emplacement. Data from boulders smaller than 80 cm have been discarded to calculate the age of M2.

4 - Description of the ice flux model of Harper and Humphrey [S3]

The 2D model of Harper and Humphrey [S3] is designed to model snow and ice flux across the landscape with a cellular automata technique. Although their approach may appear simple, as explained by Harper and Humphrey, the goal of this ice flux model is "*to strike a compromise between mass-balance models appropriate for large scales but with no representation of glacier dynamics* (i.e., [S4]) *and complex models of glacier dynamics practical only for individual glaciers or reaches of glaciers* (i.e., [S5]) *[…] The model tracks the accumulation and ablation of snow and ice, and its redistribution by glacier motion*."

Input to the model consists of (i) the landscape topography and (ii) the elevation-dependent mass-balance curve. We used here a 50 m resolution digital elevation model (DEM) of the Mauna Kea summit. The mass-balance law was calculated using the PDD-model described in the Methods section. The input DEM was transformed into a regular hexagonal lattice[3]. During a run, performed at discrete time steps, the water equivalent of snow (or ice) is added or removed to/from each grid particle according to the input mass-balance. Ice particles move within the glacier lattice synchronously, assuming ice is plastic with a yield stress of 1 bar [S6]. The glacier motion, which includes deformation and sliding within a cellule, accommodates the flux to maintain the basal shear stress at the yield stress. This plasticity criterion is a widely applied first order simplification in glacier flow modelling [S7], provided that along-glacier shear is the dominant mode of deformation. This assumption is supported by many observations and analytical evidences [S7, S8]. In addition, the validity of the model is supported by its good ability to mimic the extension of several current worldwide glaciers [S3, S9]. For this paleoclimatic study, the model was run until the modelled ice cap is in steady state and fit the LLGM moraines of Mauna Kea.

A sensitivity test was performed in order to evaluate the uncertainty associated with this dynamic model. For this, we have tested the model sensitivity to the yield stress. Considering extreme yield stress values (0.5 bar and 1.5 bar, respectively), the so-induced shift on the reconstructed temperature is ~1.3°C. Thus, it can be hypothesised that the temperature uncertainty arising from the dynamic model is ±0.7°C. For instance, this sensitivity test permits to evaluate the influence of a possible yield stress reduction during the retreat of the Pohakuloa gulch glacier after 16 ka. Such slippery bed configuration might indeed occur during warming and glacier retreat, with the net effect of a reduced yield stress.

Finally, the paleo-ELA that we infer from our modelling (3780 m for the LLGM) is consistent with the estimate of 3785±25 m proposed by Porter [S10] using the accumulation

area ratio (AAR) method. Although the AAR approach is not able to take into account a high level of topographic detail, such consistency between two different methods suggests that the assumptions of the model do not induce any significant bias in estimating the Hawaiian paleo-ELA.

5 - Calibration of the "PDD - solar radiation" model

Fig. S2 shows the agreement between the observed and the modelled mass balance of the Zongo glacier (Bolivia, 16°S) during a two years period (between 2003 and 2005). This best fit was obtained tuning the ablation parameters from least mean square optimization.

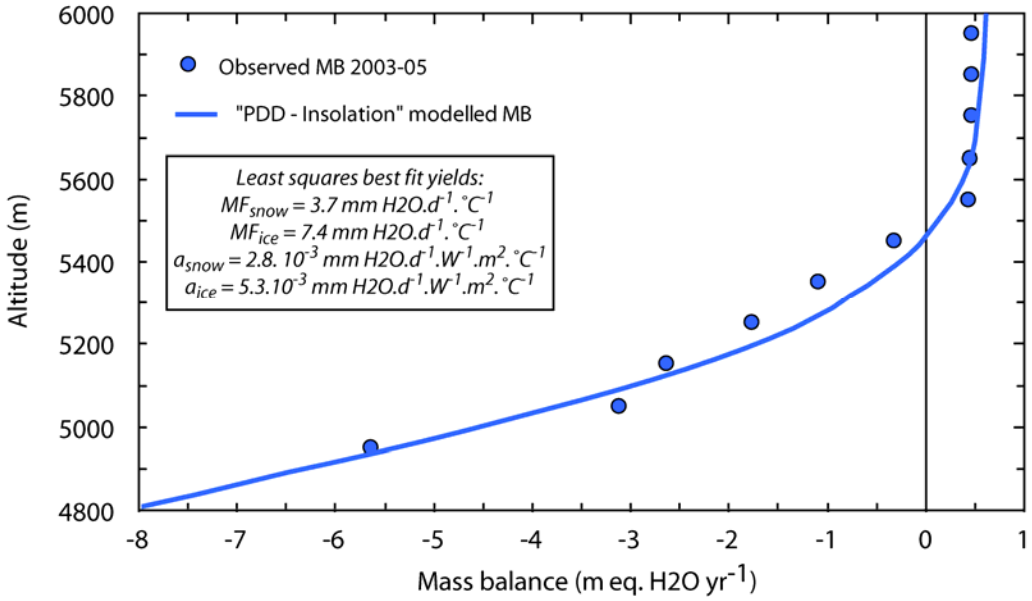

Fig. S2 - Inversion of the "PDD - solar radiation" model parameters using the 2003-05 mass balance and meteorological data from the Zongo glacier (Bolivia, 16°S)
Data from the French GLACIOCLIM network available at
http://www-lgge.ujf-grenoble.fr/ServiceObs/SiteWebAndes/index.htm

6 - Current climatic data of Mauna Kea (Hawaii, 19°N)

The climatic data presented in Fig. S3, S4 and S5 are mean value recorded during the 1970-2001 period by the Hawaiian weather stations (www.ncdc.noaa.gov). These data were inputted in our mass balance PDD model in order to estimate the temperature and precipitation variations that are necessary to reproduce the past glacier extents.

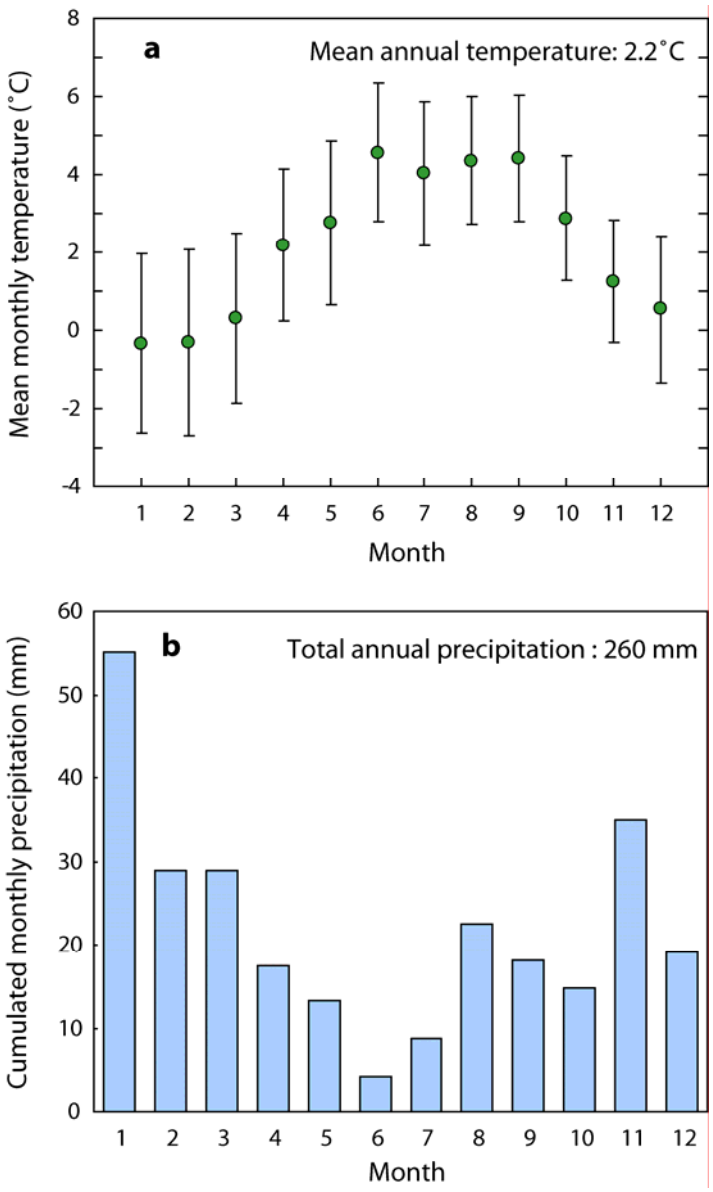

Fig. S3 - Current climatic data recorded by the Mauna Kea observatory weather station (4198 m) (www.ncdc.noaa.gov).
a - Mean monthly ground temperatures (°C).
Standard deviations varied from 1.8 (July) to 2.2 °C (January).
b - Cumulated monthly precipitation ($mm.month^{-1}$)

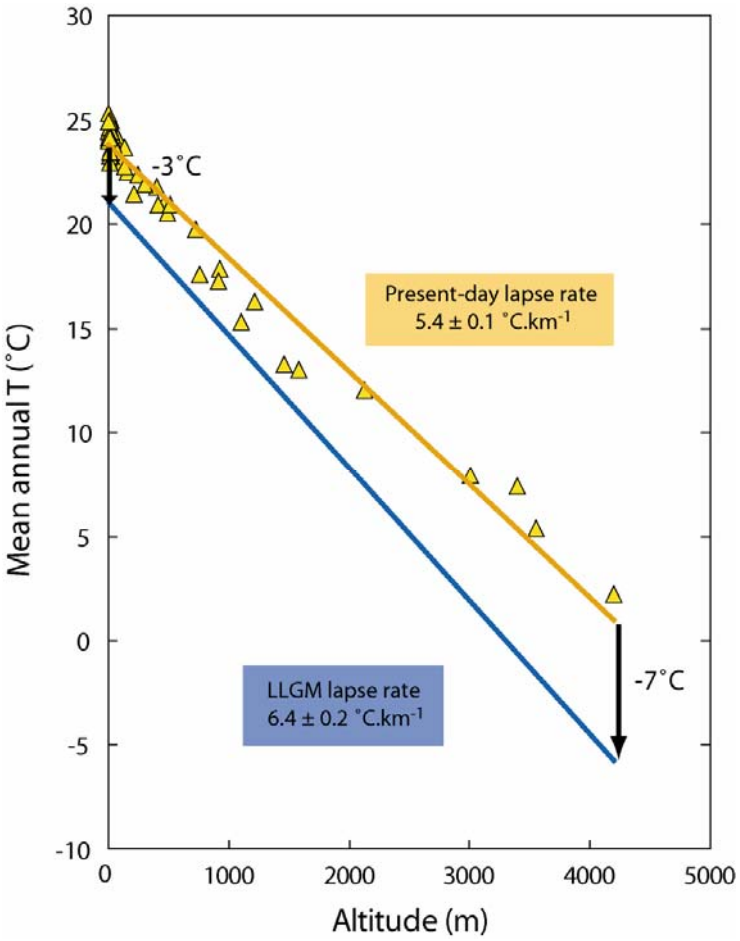

Fig. S4 - Current mean annual T (°C) *vs* altitude (m)
These data have been recorded over several years (up to 15 years between 1970 and 2001) by several Mauna Kea weather stations (www.ncdc.noaa.gov). The regression line allows a present lapse rate of 5.4±0.1°C.km^{-1} to be calculated, while the modelling proposed here requires a LLGM steeper lapse rate of 6.4±0.2°C.km^{-1} to conciliate the 7°C atmosphere cooling with the 3°C amplitude of the sea surface temperatures drop [S11].

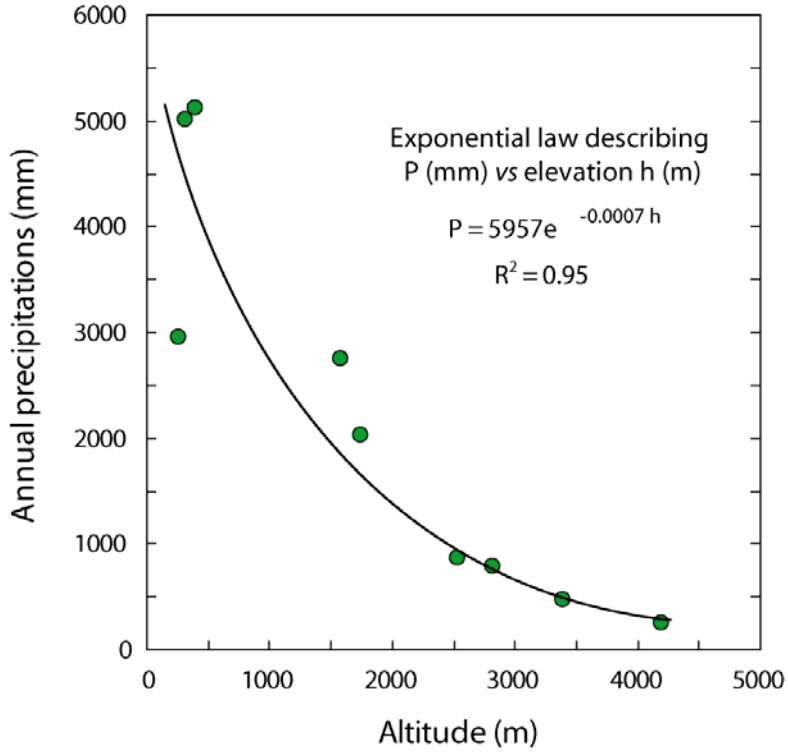

Fig. S5 - Current annual precipitation (mm) *vs* altitude (m)
These data have been recorded over 7 observation years between 1970 and 2001 by the Mauna Kea weather stations (www.ncdc.noaa.gov). The regressed exponential law is used as input in the PDD model.

7 - Evaluation of the model uncertainties

The overall uncertainty of our temperature reconstruction is ±0.9°C, assuming invariant precipitation. This imprecision arises from the uncertainty associated with the mass balance estimate (±0.5°C) and from the uncertainty of the used dynamic model (±0.7°C, see section 4). Because both sources of error can be considered as independent, we made the quadratic sum of these two uncertainties to calculate this total imprecision of ±0.9°C.

The mass balance is modelled here using monthly temperatures, precipitations, solar radiations and the local topography as input parameters. Albedo is taken into account because different melting parameters are used for snow and ice. However, the model does not treat directly other factors, such as wind velocity, relative humidity, cloudiness and sublimation, while all of these parameters may contribute in determining the ELA position [S12]. Although Mauna Kea and Zongo are both located in the Tropics at comparable distances from equator, these parameters may be different in each location. Moreover, contrary to solar radiations, accurate estimate of parameters such as wind or relative humidity are not available in the past.

As argued by [S13], the reported variations of the calibrated PDD parameters from an area to another are likely resulting from regional differences and particularly those linked to humidity, wind speed and cloudiness changes. Consequently, a sensitivity test can be used to establish the uncertainty arising from the meteorological parameters. For this, we used extreme values for MF and a (×0.7 to ×1.3, that is the reported range for tropical glaciers [S13]) to evaluate the maximum bias that would be induced by a significant variations of any parameters (Fig. S6). This test was performed using the Zongo glacier mass balance. The results show that extreme variations of melting parameters would not induce an ELA shift higher than ~100 m. Consequently, assuming a lapse rate of 6.5°C/km, the bias on the deduced temperature change would remain below 0.7°C.

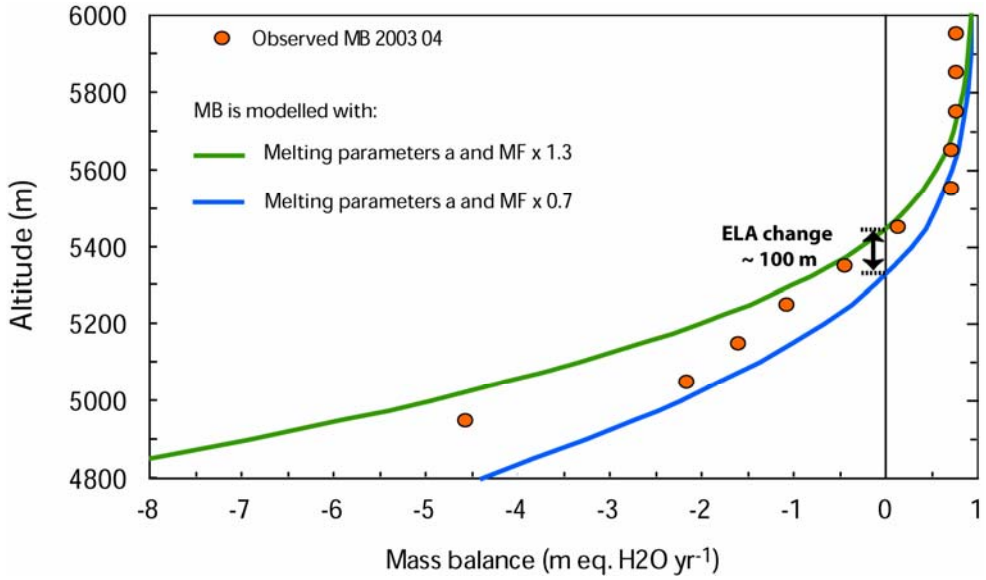

Fig. S6 - Sensitivity of the modelled MB to the melting factor values (Zongo glacier, 2003-04 data)

In order to assess the uncertainty of our conclusions, the same approach was used to reconstruct the paleoclimate of Hawaii (Fig. 3c). It has to be noted that the 0.7°C uncertainty associated with the ice flux model was also taken into account to determine the blue shaded area (Fig. 3c) which represents the confidence interval of the climatic reconstruction. This corresponds to a total temperature uncertainty of ±0.9°C, assuming invariant precipitation.

We also addressed the influence of temperature seasonality. For this, we have tested the sensitivity of our paleoclimatic reconstruction for different seasonal amplitudes. The test shows that, when temperature seasonality is lowered to 2°C (while the current amplitude between summer and winter is 4°C, Fig. S3a), a cooling of ~6.3°C is required to reproduce the LGM glacial extent. Such value remains compatible with the ~7°C cooling that is inferred

assuming the seasonality is 4°C. Moreover, proxies of seasonal SST [S14] do not show any change in seasonality between the LGM and today in the central Pacific. Proxies of atmosphere temperature (noble gases and pollen assemblages) lead to the same conclusion for tropical lands [S15]. This stability between present day and LGM conditions is due to the low variations in insolation in the tropics, which offers little scope for seasonal changes in temperature [S15]. Because of these observations, it is quite firm to assume that the LGM seasonality in Hawaii was similar than today.

Finally, the model accuracy can also be evaluated observing the climatic conditions at the ELA for several tropical glaciers. This comparison shows that a first order correlation can be established between the summer temperature and the annual precipitation at the ELA (Fig. S7).

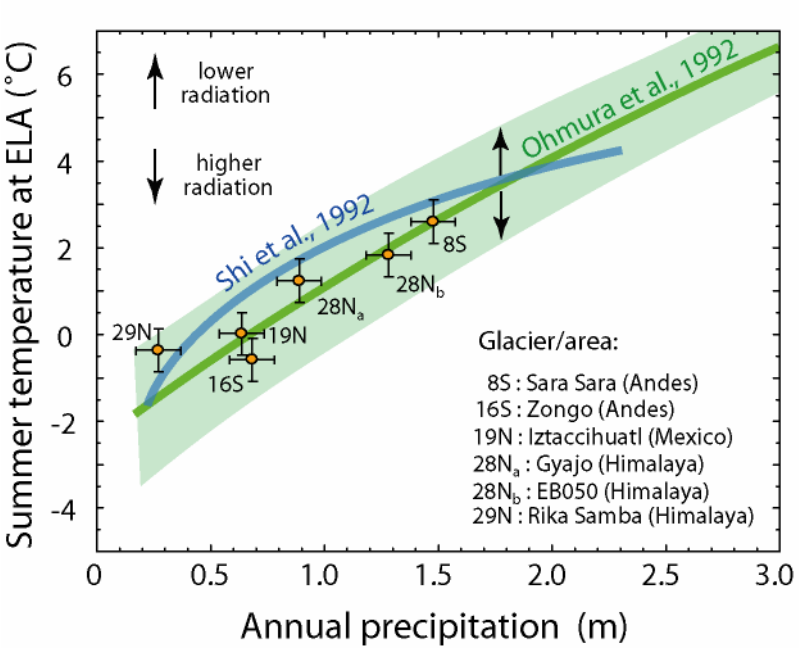

Fig. S7 - Annual total precipitations and mean summer ground temperature at the ELA
The empirical law of Ohmura et al. (1992) [S16] (green area) is deduced from 70 worldwide glaciers. The empirical relationship of Shi et al. (1992) [S17] (blue line) is determined from 16 Himalayan glaciers.
Orange points are calculated (this study) using the ELA database of Mark et al. (2005) [S18] and climatic data from the www.worldclimate.com database.

Although these relations are not obtained using a precise mass balance gradient such as the one monitored on the Zongo, this plot demonstrates that temperatures and precipitations are correlated at the ELA, within uncertainties, whatever the tropical area, and whatever the values of local parameters such as relative humidity, wind or cloudiness. It is important to

highlight that, in the tropics, for a given precipitation value, the range of the temperature variations at the ELA is not higher than 2°C. Variations in net radiations are the principal cause of this temperature scattering [S16]. However, temporal and spatial changes in radiation are taken into account in our model (at least partially) because it includes an independent estimate of insolation in Hawaii since the local LGM. This observation is another argument supporting the accuracy of the ±0.9°C uncertainty associated with the paleotemperature reconstruction.

References used in Supplementary information

S1. Wolfe, E. W., Wise, W. S. & Dalrymple, G. B. The geology and petrology of Mauna Kea volcano, Hawaii - a study of postshield volcanism. *U.S. Geological Survey professional paper* **1557** (1997).

S2. Brown, E. T., Molnar, P. & Bourles, D. L. Comment on "Slip-rate measurements on the Karakorum Fault may imply secular variations in fault motion". *Science* **309**, doi: 10.1126/science.309.5739.1324a (2005).

S3. Harper, J. T. & Humphrey, N. F. High altitude Himalayan climate inferred from glacial ice flux. *Geophysical Research Letters* **30**, 1764-1767 (2003).

S4. Hostetler, S. W. & Clark, P. U. Tropical climate at the last glacial maximum inferred from glacier mass-balance modeling. *Science* **290**, 1747-1750 (2000).

S5. Blatter, H. Velocity and stress-fields in grounded glaciers - a simple algorithm for including deviatoric stress gradients. *Journal of Glaciology* **41**, 333-344 (1995).

S6. Nye, J. F. The flow of glaciers and ice-sheets as a problem in plasticity. *Proceedings of the Royal Society of London series a - Mathematical and Physical Sciences* **207**, 554-572 (1951).

S7. Paterson, W. S. B. *The physics of glaciers* (ed. Elsevier) (Tarrytown, New York, 1994).

S8. Bahr, D. B., Meier, M. F. & Peckham, S. D. The physical basis of glacier volume-area scaling. *Journal of Geophysical Research - Solid Earth* **102**, 20355-20362 (1997).

S9. Blard, P.-H., Wagnon, P, Lavé, J. & Sicart J.-E. Calibration of a degree day model for tropical glaciers using mass balance data from the Zongo glacier (Bolivia, 16°S). *Journal of Hydrology* (in prep).

S10. Porter, S. C. Pleistocene snowlines and glaciation of the Hawaiian Islands. *Quaternary International* **138**, 118-128 (2005).

S11. Lee, K. E., Slowey, N. C. & Herbert, T. D. Glacial sea surface temperatures in the subtropical North Pacific: A comparison of U-k(37)', $\delta^{18}O$, and foraminiferal assemblage temperature estimates. *Paleoceanography* **16**, 268-279 (2001).

S12. Kaser, G. Glacier-climate interactions at low latitudes. *Journal of Glaciology* **47** (2001).

S13. Hock, R. Temperature index melt modelling in mountain areas. *Journal of Hydrology* **282**, 104-115 (2003).

S14. Lee, K. E. & Slowey, N. C. Cool surface waters of the subtropical North Pacific Ocean during the last glacial. *Nature* **397**, 512-514 (1999).

S15. Farrera, I. et al. Tropical climates at the Last Glacial Maximum: a new synthesis of terrestrial palaeoclimate data. I. Vegetation, lake levels and geochemistry. *Climate Dynamics* **15**, 823-856 (1999).

S16. Ohmura, A., Kasser, P. & Funk, M. Climate at the equilibrium line of glaciers. *Journal of Glaciology* **38**, 397-411 (1992).

S17. Shi, Y. Characteristics of late Quaternary monsoonal glaciation on the Tibetan Plateau and in East Asia. *Quaternary International* **97-8**, 79-91 (2002).

S18. Mark, B. G. et al. Tropical snowline changes at the last glacial maximum: A global assessment. *Quaternary International* **138**, 168-201 (2005).